Off-Axis Telescopes for Dark Energy Investigations

Michael L. Lampton[1], Michael J. Sholl[1], and Michael E. Levi[2]

[1]University of California Space Sciences Laboratory, Berkeley CA 94720 USA
[2]Lawrence Berkeley National Laboratory, Berkeley CA 94720 USA

ABSTRACT

It is well known that a telescope with an unobstructed circular pupil delivers a smaller diffraction pattern than one centrally obstructed by its secondary mirror. Spaceborne dark energy investigations require measuring targets over a wide range of redshifts, with the most distant galaxies being the reddest, faintest, and smallest. For any given signal-to-noise (SNR) requirement, these highest redshift targets are the most demanding in terms of mission cost (time, aperture, etc), not only because they are faint but also because the diffraction pattern is largest at the longest wavelengths being observed. At the same time, a telescope's field of view must be large -- the order of a square degree -- to survey the entire extragalactic sky in reasonable time. The large field of view imposes a minimum requirement on the size of the secondary mirror baffle. For a centrally obstructed telescope, an enlarged secondary mirror baffle further enlarges the diffraction pattern. Previously published JDEM telescopes were centrally obstructed. Here, we explore unobstructed telescope designs because these can have a nearly ideal Airy diffraction pattern, avoiding both the central obstruction and the supporting spider legs, limited only by optical manufacturing and alignment errors. They therefore can deliver the best possible SNR for a given aperture. Simulations show that a 1.1m unobstructed aperture can deliver about the same cosmological constraints as a 1.4m aperture that has a 50% linear central obstruction.

Keywords: three-mirror telescopes, unobstructed pupils, space astronomy, dark energy, wide-field imaging
Contact: mlampton@ssl.berkeley.edu

1. DARK ENERGY and JDEM

The discovery of accelerated expansion of the universe by Perlmutter et al.[1] and Riess et al.[2] has triggered a worldwide effort to understand the physics behind this unexpected behavior. A variety of proposed observational techniques have emerged to constrain dark energy via astronomical measurement. Three of the most promising techniques include the use of Baryon Acoustic Oscillations (BAO), Type 1a Supernovae (SNe) and gravitational Weak Lensing (WL). Each technique requires an extensive survey of targets, spanning a cosmologically significant range of redshifts, and each technique benefits from the use of ground-based and spaced observatories. A mechanism to help quantify the usefulness of a proposed measurement set was developed by the Dark Energy Task Force[3], whose findings have helped guide program planning. A variety of potential dark energy space missions, including the Joint Dark Energy Mission (JDEM), are compared in Sholl et al.[4] and in Content et al.[5]

To give an impression of the observing tasks involved, in Figure 1 we show a typical observing situation for a supernova program: a signal-to-noise spectrum in the near infrared showing the features exhibited by supernovae of type Ia, which is the best type to use as a calibrated standard candle. The spectrum is crucial for classification, for redshift determination, and for magnitude. By combining a thousand or more supernovae over a range of cosmologically significant distances, the luminosity distance relationship (the Hubble diagram) of the Universe can be constrained.

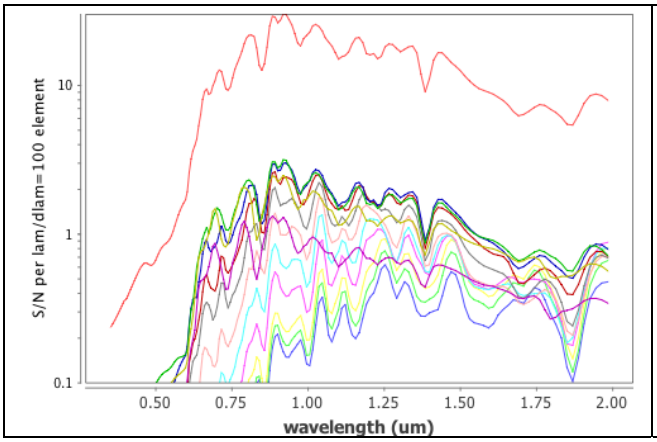

Figure 1: Distant supernovae reveal their classification types and their redshifts by their spectra. Here, a typical signal/noise plot is shown for a type Ia supernova at redshift z=1.3. Top curve (red) is for a deep exposure at maximum light, delivering high signal to noise ratio for accurate registration of individual features; other curves represent shorter exposures taken earlier and later, to follow the shape of the light curve and the evolution of the colors of the supernova. Figure courtesy of A.G.Kim (private communication 2010).

In Figure 2 we show a schematic slitless dispersed image of the sky in the near infrared. With a wide field telescope, thousands of emission line galaxies are harvested in each exposure and over the course of a one or two year program a highly detailed history of the galaxy correlation function can be constructed.

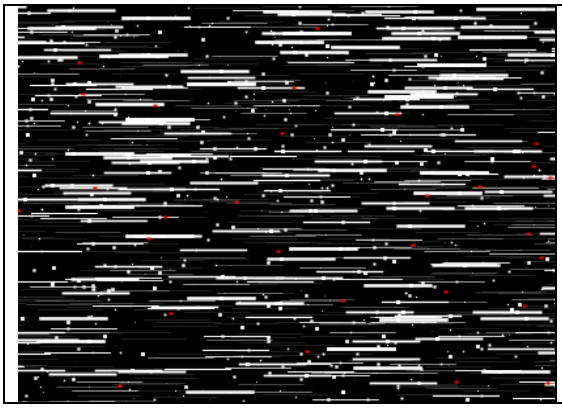

Figure 2: BAO objective: a slitless prism image of the sky in the near infrared. Stars and galaxies are dispersed over a wavelength range defined by a bandpass filter. Each emission line galaxy is revealed by the presence of one or more bright spots along the length of its spectrum. In most cases the brightest line is the hydrogen Halpha line at 0.6563 microns, redshifted into the near infrared. The observing goal is to survey 16000 square degrees of sky, yielding ~ 50 million galaxies, with redshift error < 0.001(1+z), to determine the galaxy correlation function and its evolution over cosmic time.

In Figure 3 we illustrate power of the weak lensing principle to map a distant mass concentration.

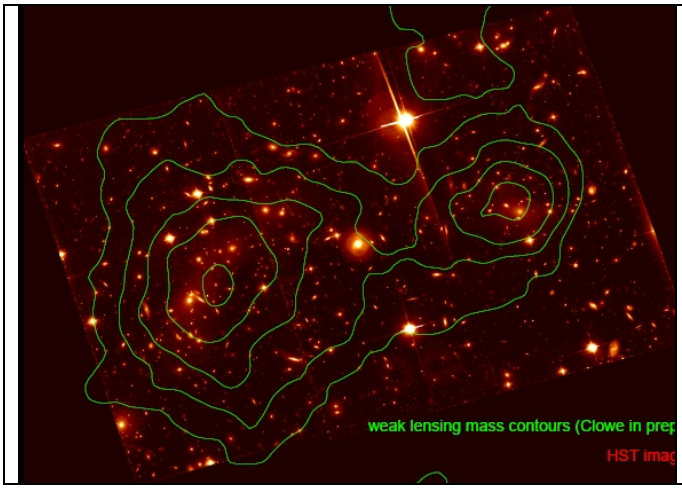

Fig. 3. Gravity deflects light from background galaxies and also alters the shear, or deviation from roundness, that those galaxies appear to have. Shear maps can be deconvolved to yield mass distributions along the line of sight. The Bullet cluster serves as an example of the extraction of an isolated mass distribution from a collection of shear measurements on background galaxies. (HST file image, courtesy NASA.) The key finding of these studies is that WL mass mapping demands a high density of galaxies that are resolved, not merely detected. This in turn requires a small PSF and a fine pixellization.

Here, the systematic variations in observed ellipticity of galaxies reveal the foreground mass distribution within the Bullet cluster. For cosmology, a key diagnostic of the growth of structure in the evolving universe would be obtained if weak lensing measurements could be extended to a very wide survey with a high density of *resolved* galaxies distributed over a cosmologically significant redshift range. These galaxies are small (0.1 to 0.2 arcsec half-light radius), so high angular resolution is mandatory.

JDEM's scientific objectives were prioritized by a Science Coordination Group in 2008-2009 and are being further defined by an Interim Science Working Group whose first report[6] was published this year. The goal of these efforts is to determine the most cost-effective way to pursue the study of Dark Energy, within limitations of likely project funding constraints and in view of other likely programs, both ground- and space-based. Working with the JDEM project offices at NASA and DoE, the ISWG quantified two alternative JDEM mission scenarios: Design A, performing a BAO survey and a SN survey, and a more complex but less detailed Design B capable of conducting all three objectives (BAO, SNe, and WL). These designs are detailed in Content et al.[5] and Sholl et al.[7] We summarize these two JDEM designs as they presently stand: Table 1 lists the broad science objectives and Table 2 lists the major science payload elements. Both designs emphasize wide-field surveys in the near infrared, since the NIR is by far more accessible from space than from mountaintop observatories. Continuing definition work will surely lead to improvements in mission performance and improved understanding of mission cost and schedule. In this paper, we discuss the considerations that have led us to select a relatively unusual telescope configuration, the unobscured-pupil three-mirror anastigmat (TMA) layout.

Table 1: JDEM Science Objectives[6]

Science Objective	Design A	Design B
Supernova Redshift Survey	1500 supernovae Redshifts $0.2<z<1.5$ Tiered survey areas for discovery	Same as Design A
BAO Galaxy Survey	Halpha flux 2e-16 erg/cm2sec Spectroscopic redshifts $1.3<z<2.0$ RMS $z < 0.001\cdot(1+z)$ 16000 square degrees in 1.5 years	Same as Design A
Weak Lensing Survey	none	10000 square degrees 30 galaxies per square arcminute Redshifts from Photo-Z 1e5 spectro calibration galaxies

Table 2: JDEM Payload Elements

Element	Design A	Design B
Telescope	1.1m unobscured aperture TMA	Similar to A
Wide field imager For BAO centroids For SN discovery searches In Design B, for cosmic shear	0.5 square degree FoV Two bands: 0.7-1um, 1-1.5um 32 Mpixels, each 0.45arcsec HgCdTe 2Kx2K	Similar to A Similar to A More & finer pixels HgCdTe and/or Si CCD
Slitless prism spectrometer For BAO galaxy redshifts	0.5 square degree FoV One waveband 1.5 – 2.0 um 32 Mpixels, each 0.45arcsec	Similar to A Similar to A Similar to A
Supernova Slit orIFU spectrometer Light curves, spectra, host redshifts	Narrow field (a few arcseconds) One waveband 0.4 – 2.0um	Similar to A Similar to A

2. MISSION DESIGN CONSIDERATIONS

The major contrast between dark energy missions and traditional space observatories is the need to survey large sky areas efficiently. The sky survey rate depends linearly on the instrument field of view (FoV):

$$\text{SurveyRate} = \text{FoV} / \text{Texposure}$$

Exposure time requirements depend on properties of the target, the sky background level, and the optical train including sensor pixels. The simplest case -- continuum source, sky noise dominating target noise and sensor noise – will serve to illustrate the system-level optical trades. Let Nmin represent the continuum photon flux of the faintest required targets, and let SNR represent the required signal-to-noise ratio. Let A represent the telescope aperture area, let E be the optical throughput efficiency, and let F be the fraction of on-orbit shutter-open time devoted to a given scientific objective. For a given continuum sky photon brightness B and a given wavelength bandpass $\Delta\lambda$, let $\Omega = \pi r^2$ represent the sky solid angle of the image spot that contains half the target flux (including target size, optical PSF, and pixellization broadening) and r = half energy radius angle. Then:

$$\text{Texposure} = 4\,(\text{SNR}/\text{Nmin})^2\,(\pi r^2\,\text{B}/\text{AEF}\,\Delta\lambda)$$

whereupon

$$\text{SurveyRate} = 0.25\,\text{Nmin}^2/(\text{SNR}^2\,\text{B}) \bullet \text{FoV A E F}\,\Delta\lambda / \pi r^2$$

In this expression the first group of factors is fixed entirely by the target objectives and the sky environment, while the second group is largely set by the payload and its operations plan. The image half-energy solid angle πr^2 is of course determined by both. This short derivation makes it clear that mission factors that increase r unnecessarily are very costly to the survey rate, because r enters *squared* in the denominator.

3. JSIM

Although simple formulations such as the above can motivate payload trade studies, actual mission planning requires a fully developed model of signal-to-noise ratios under a variety of observing conditions. BAO emission line redshift determination, for example, imposes its own requirements for roll maneuvers and wavelength zero-points. When large sky surveys are anticipated, the distribution of zodiacal light levels over the sky must be considered. The instrumental PSF is dependent on wavelength, and the distribution of galaxy sizes influences the mission trade outcomes. JSIM[8] is a mission simulator created by the Peoject Offices that includes galaxy distributions from the zCOSMOS survey, an MTF formalism to describe the system optics & sensors, and a noise model that includes zodiacal light and sensor noise. It has proven useful in estimating the productivity of a host of alternative JDEM configurations including BAO, SNe, and WL. JSIM predicts that a 1.1 m unobscured pupil delivers about the same cosmology as a 1.4 m telescope that is 50% linearly obscured (i.e. 25% of its area is blocked).

JDEM's evolution has increasingly emphasized the near infrared wavelengths (longward of one micron) that are less accessible from mountaintop observatories, but where targets are more highly redshifted – hence fainter – and where pupil diffraction becomes the major contributor to πr^2. At the same time cost constraints argue against increasing the telescope primary mirror size. Focal plane costs and telemetry load increase with pixel count, which in turn is proportional to FoV/ πr^2; yet this ratio also directly contributes to the survey rate. Consequently the telescope engineer's job is to do more with less: deliver a

wide-field image with the smallest practical diffraction pattern using an optical train whose size, mass, and complexity is limited.

4. PUPIL DIFFRACTION

The diffraction pattern of a circular pupil is the well-known Airy pattern, a central peak surrounded by a collection of rings (see for example Born and Wolfe[9] or Schroeder[10]). In Fig 4 below we show the contrast between the ideal diffraction pattern of an unobscured pupil and the 50% linearly obscured case. Unlike the customary PSF diagrams that always have unit peak, here we show the reduction in peak height due to both blockage and diffraction. It is qualitatively clear that a given target will have a higher signal to noise ratio and be better resolved in the unobscured image both because its peak is higher and its diffraction rings are fainter.

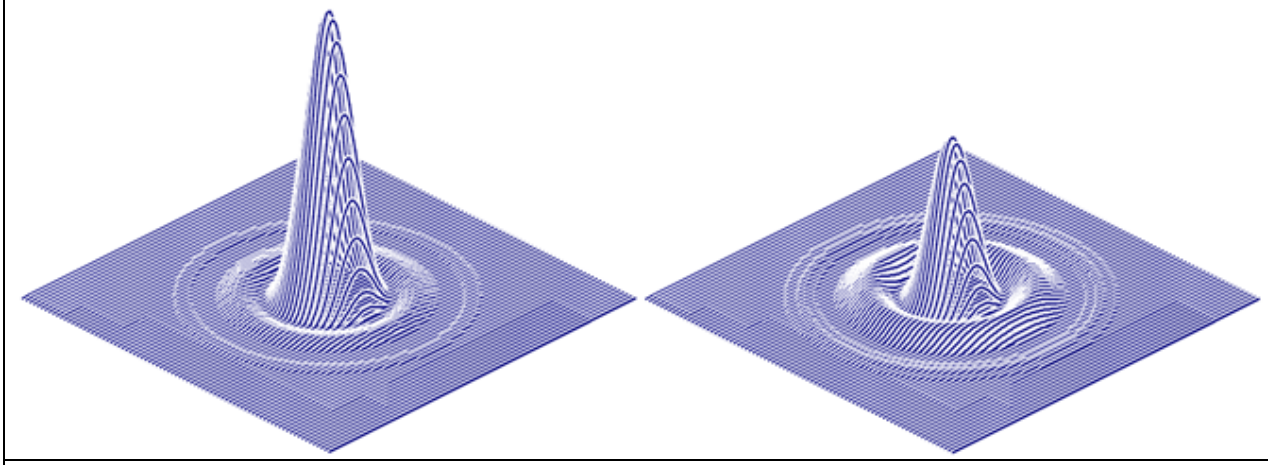

Fig 4: Monochromatic Fresnel-Kirchoff diffraction of a circular pupil. Left: no obstruction. Right: 50% linear obstruction (25% area blocked). Figures are vertically scaled for equal incident flux.

A useful characterization of the pupil diffraction is the dependence of encircled energy (EE) on image radius. What is not widely appreciated is the relatively severe loss of EE that is caused by a central obstruction of the pupil caused by an axisymmetric secondary mirror and its associated stray light baffle. On a narrow field telescope like HST, the linear obscuration can amount to 33% of the pupil diameter, and on a wide field survey telescope it can exceed 50%. In Figure 5 we plot EE vs image radius for an unaberrated pupil at several linear obscuration ratios.

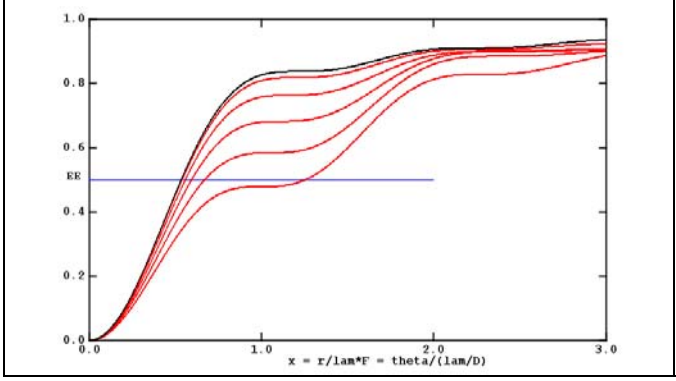

Fig. 5: Encircled energy vs radius (here in units of lambda/Fnumber) for an ideal circular pupil with central linear obscurations of 0, 10, 20, 30, 40, and 50%. The radius for the EE=50% level grows rapidly as the obstruction size approaches half the pupil size. Target size, aberrations, manufacturing tolerances and guiding errors further reduce the EE.

The deleterious effects of enlarged pupil diffraction on JDEM science are twofold. First, there is an immediate loss of signal to noise ratio because a larger amount of diffuse sky illumination (chiefly zodiacal light, even at high ecliptic latitudes) becomes mingled with the target photons. This effect is most severe on the smallest targets, which are generally the most distant galaxies and hence the faintest. Second, there is an immediate loss of spatial resolution that limits the system's ability to resolve ellipticity on the smaller and more distant galaxies, which in turn limits the cosmological reach of a weak lensing survey.

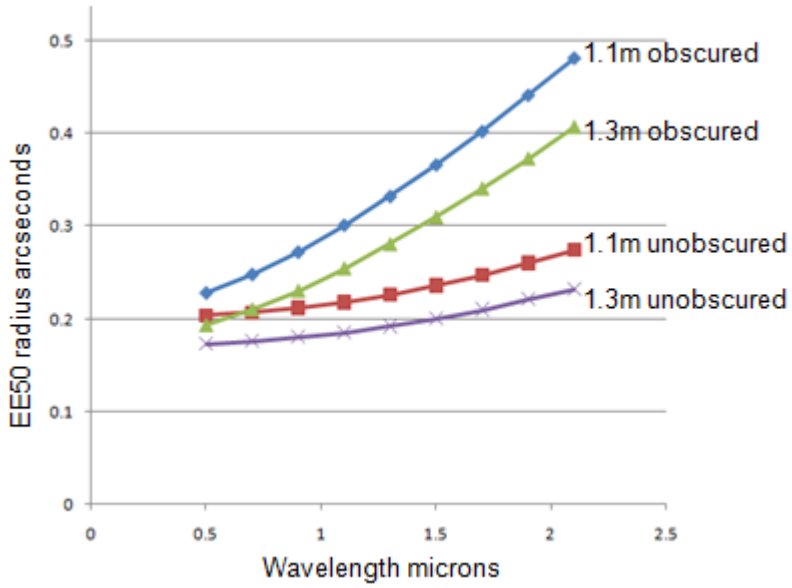

Fig. 6: A telescope's EE50 radius is determined by a number of factors including aberrations, optical manufacturing errors, alignment, pixellization, and attitude control system jitter. At increasingly long wavelengths, where signal-to-noise ratio is most demanding, diffraction can easily dominate the PSF curve, particularly for smaller telescope apertures.

5. SPIDERS

A secondary mirror (SM) at center of a pupil requires stable mechanical support, customarily provided by a structure connecting the SM to rest of the telescope. The legs of this structure obstruct light and complicate the diffraction pattern. The monochromatic diffraction pattern for the unobscured pupil is contrasted with the pattern for a pupil having a three legged spider and a 50% central circular obstruction in Figure 7. The vertical scale is logarithmic, spanning four orders of magnitude. The obstructions make the ring pattern more irregular, and at larger distances from the central star, the leg diffraction spikes dominate.

For telescopes like JDEM whose survey speed is directly limited by the level and smoothness of the foreground Zodiacal light, it's important to keep the diffraction features far below the Zodiacal light level over as much of the sky as possible. Minimizing the ring energy, and eliminating the spike energy, both help this effort.

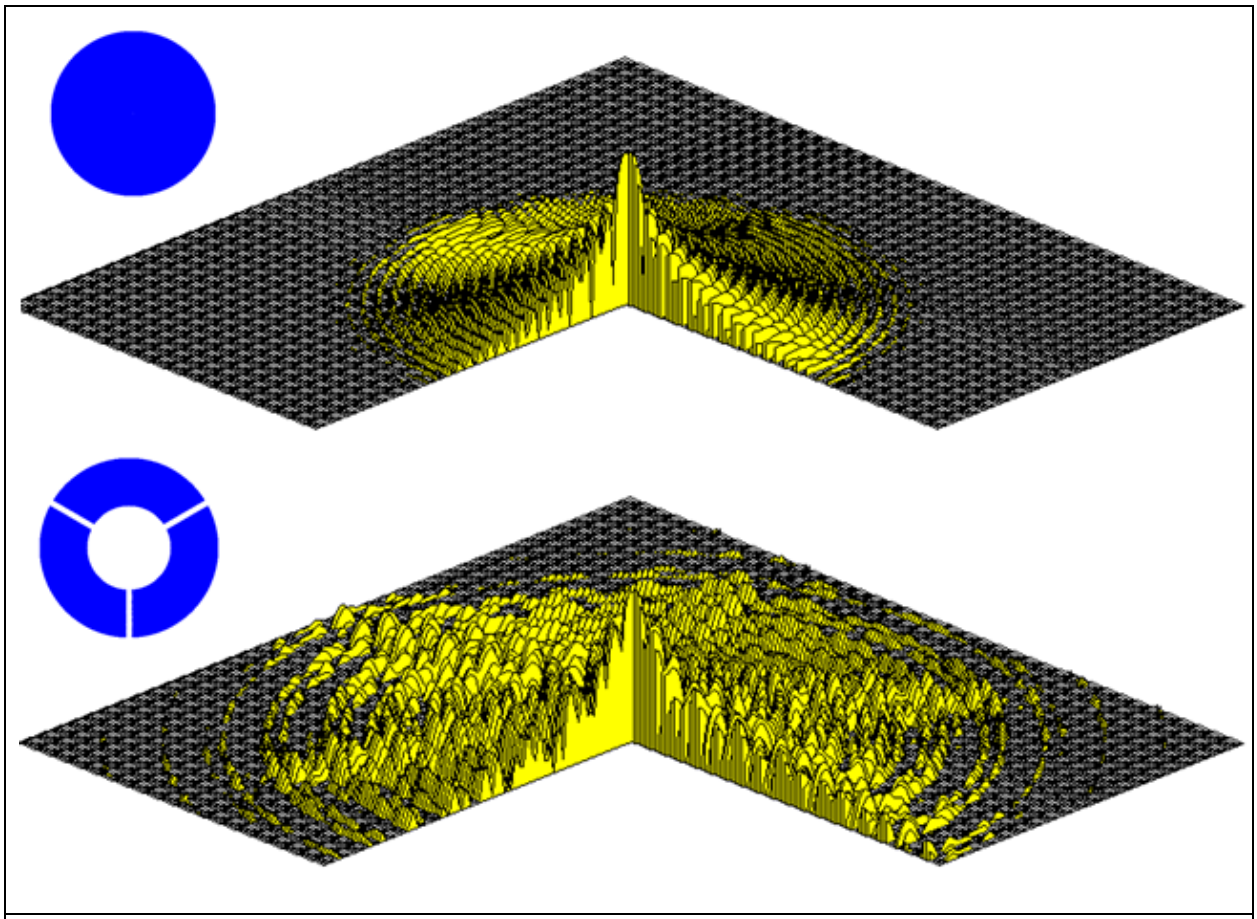

Figure 7: Monochromatic diffraction for unaberrated pupils. Top: an unobscured pupil. Bottom: pupil obscured by a centered 50% linear disk and three spider legs. Pupils are shown at the upper left. Logarithmic vertical scale spans four decades. Fresnel-Kirchoff diffraction assumed.

6. UNOBSCURED TELESCOPES, GROUNDBASED AND SPACEBORNE

Telescopes with unobscured pupils are unusual in space astronomy, although they have been in routine use for remote sensing applications and elsewhere. In Table 3 we list some existing and proposed unobscured telescope designs.

The motives for adopting an unobscured pupil depend entirely on the application. For solar telescopes, it is impractical to have a secondary mirror due to the extreme heat load of concentrated sunlight, and it is therefore customary that the solar image be formed at a very long prime focus and a correspondingly slow f/number. In spaceborne remote sensing, flight packages usually have to be very compact yet deliver good contrast at ground resolutions of the order of one meter; the unobscured option has improved contrast owing to its superior modulation transfer function (MTF) curve. In spaceborne planetary searches, the central issue is minimizing the glare from the parent star, which in turn is aided by the reduced diffraction energy at angles of the order of an arcsecond, 10 or 20 rings out.

Table 3: Unobscured Telescopes and Concepts

Mountaintop	Solar	McMath: Pierce[11] NST: Denker et al.[12] ATST: Rimmele[13]
Mountaintop	General Astronomy	LAPCAT (proposed): Storey et al[14] NPT (proposed): Moretto & Kuhn[15] 4m DFL (proposed): Moretto & Kuhn[16]
Spaceborne	Remote Sensing	MTI: Kay et al.[17] TopSat: Price[18] QuickBird: Figoski[19] EO-1 ALI: Lencione et al[20] CartoSat: Subrahmanyam et al[21]
Spaceborne	Stellar	GAIA: Perryman[22] DIVA (proposed): Graue et al[23]
Spaceborne	Planet Search	JPF (proposed): Krist et al[24] TPF (proposed): Noecker[25] ECLIPSE (proposed): Trauger et al[26], Hull et al[27]

We should also acknowledge the many other more general unobscured telescope concepts and mathematical treatments that have been presented[28-36] in a variety of contexts.

7. THREE MIRROR ANASTIGMATS (TMAs)

Telescopes that must deliver a wide diffraction-limited field of view, and also deliver a telephoto advantage factor considerably greater than 1, are generally TMAs (Lampton and Sholl[37]; Sholl et al.[38]). The two principal categories of TMA are those that derive from the Korsch[39] centrally obscured layout, and those that derive from the Cook[40] unobscured design. These are shown in Figure 8. The specific features that the TMA offers for astronomical surveying are (1) the availability of a field stop for tight control of stray light, (2) a real exit pupil for control of stray heat, (3) a significant telephoto advantage allowing a long focus optical train to be packaged in a compact payload envelope, and (4) a highly flexible range of available plate scales to accommodate a range of mission requirements.

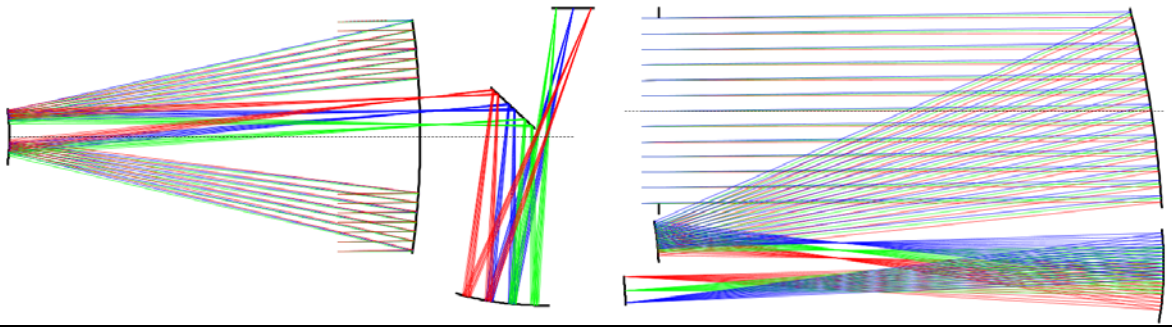

Fig. 8: (Left) a Korsch[39] type eccentric-field TMA telescope. (Right) a Cook[40] type off-axis TMA telescope. Both types have an accessible field stop for control of stray light and an accessible exit pupil for control of stray heat. The Cook TMA has an unobstructed pupil. For the same aperture, this gives the Cook a larger light gathering area and a smaller diffraction pattern. These historical examples are both focal, but afocal variants are equally practical and may be advantageous for JDEM.

8. ADOPTING UNOBSTRUCTED PUPILS

Difficulties in manufacturing off-axis aspheres and alignment of off-axis and eccentric field TMAs were the main obstacles to their implementation in practical systems when these forms were introduced in the late 1970s. Today, numerous optic suppliers are capable of manufacturing, testing, and aligning off-axis aspheric telescopes, and a number of examples are already flying. With computer-controlled machining equipment and figuring engines, one may manufacture the off-axis mirror directly, without first creating the parent optic and then cutting out the desired off-axis section. For space flight applications, the primary mirror is typically manufactured with a lightweight rib structure, whose stiffness, strength, and stability are improved with continuous load paths across the backside of the mirror. Of course these qualities are further improved with a reduction in mirror outer diameter.

When compared with an on-axis Korsch-type TMA, an off-axis design has certain penalties. The spacing between the primary and secondary mirrors is driven by geometric blur and the size of the parent optic, not the actual diameter of the mirror. For example, spacing from the secondary mirror from a 1.1m on-axis primary mirror is about 1.3m, while the same diameter off-axis primary mirror would be separated 2.4m from the secondary mirror. This typically leads to less-efficient packaging of an off-axis TMA when compared to an on-axis TMA having the same primary mirror diameter. A tightly constrained payload envelope can be set a serious constraint on mirror size. Of course, packaging depends on the specifics of a given telescope and instrument suite, and scenarios do exist in which an off-axis telescope can be efficiently laid out. For example, JDEM requires its sensor packages to be passively cooled, which is simplified if these are located alongside the telescope on its antisunward side.

Manufacturing of off-axis mirrors is more complex than those of an obscured telescope, both because the mirrors are not axisymmetric, and because the departure from a sphere (aspheric departure) is several times higher on an off-axis telescope than that of a similar on-axis mirror. Figure 9 shows aspheric departure of 1.1m diameter on-axis and off-axis TMA primary mirrors. Aspheric departure relates directly to polishing time, and an off-axis primary mirror can consequently require a longer lead-time for procurement when the mirror manufacturer starts with a spherical surface.

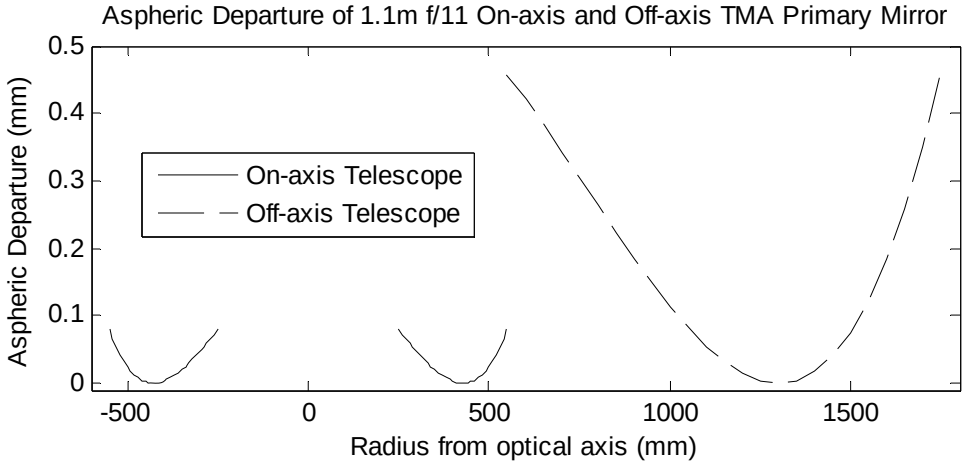

Figure 9: Aspheric departure of an off-axis primary mirror is several times larger than an on-axis mirror.

9. SPECIFIC JDEM IMPLEMENTATION TRADES

To proceed into mission definition, a clear statement of requirements is mandatory. Every optical design expresses the results of a series of trade studies, many of which are continuing to be studied at both JDEM project offices. An obvious trade is the choice of focal length(s) and corresponding plate scales: what choice delivers the best cosmological constraints? It is certain that the best choice(s) will depend on the emphasis given to the scientific objectives.

Another key trade is the choice between a focal telescope and an afocal telescope equipped with one or more cameras. The use of two or more cameras allows specific focal lengths to be chosen for each observing field, but may increase the mission hardware cost. Alternatively, a focal telescope can be fitted with beamsplitters and or focal reducers/increasers and still have a useful, but smaller, range of flexibility.

A related trade affecting the optics is the choice of sensor pixel sizes. As a general rule, the optical PSF grows with wavelength, and if detectors were specialized by wavelength, their pixel scales could serve to match the PSF even with a common plate scale. An aspect of this trade is the issue of sampling and aliasing. For simple flux surveys, coarse pixel scales roughly matched to the PSF are adequate, but to distinguish galaxy shapes for shear determination or other science, a finer scale is mandatory. Dithering (see for example Bernstein[41]) can substitute for finer pixels at some level but simulation work will be needed to identify the best tradeoff.

For a given architecture, the detailed engineering work of establishing fields, biases, tolerances, wavefront error budgets, and integration/test flow can begin. For JDEM such work has already started and is reported on by Content et al.[5] in these proceedings.

10. CONCLUSIONS

The architecture of the JDEM observatory is driven by the demands of the three baselined techniques: Baryon Acoustic Oscillations, Supernovae, and Weak Lensing. BAO and SN discovery surveys can be conducted using a coarse pixel scale and a short focal length, and benefit from rapid sky coverage. Supernova spectroscopy will require a rather fine pixel scale, carefully optimized against the overall PSF size to maximize the signal to noise ratios for the faintest targets. Weak Lensing surveys require a large working field of view but also a relatively fine pixel scale to resolve galaxy ellipticity to redshifts beyond 2.0. Ancillary science objectives would for the most part also benefit from fine pixel scales. The adoption of an unobscured pupil may slightly complicate the fabrication and test of the JDEM telescope but will deliver an improved signal to noise ratio on all but the largest target galaxies, compared to a centrally obstructed telescope. Mission simulations show that a 1.1m unobscured pupil is comparable to a 1.4m pupil that is 50% linearly obscured, in terms of the survey rate yielding a given signal to noise ratio over a mix of JDEM targets.

ACKNOWLEDGMENTS

This work was supported by the Director, Office of Science, of the U.S. Department of Energy under Contract No. DE-AC02-05CH11231.

REFERENCES

[1] Perlmuttter, S., et al., Ap.J. **517,** 565-586 (1999).
[2] Riess, A., et al., A.J. **116,** 1009-1038 (1998).
[3] Dark Energy Task Force Final Report, http://www.NSF.gov/mps/ast/detf.jsp (2006).
[4] Sholl,M., et al., Proc SPIE **7436,** #03 (2009).
[5] Content, D., et al., this conference (2010).
[6] JDEM ISWG "Report to NASA and DOE Headquarters, http://jdem.lbl.gov (2010).
[7] Sholl, M., et al., this conference (2010).
[8] JDEM Mission Calculator, http://jdem.lbl.gov/public/etc/jsim.html (2010).
[9] Born,M., and E. Wolf, "Principles of Optics," Cambridge University Press 7th Edition (1999).
[10] Schroeder, D.J., "Astronomical Optics," Academic Press 2nd Edition (2000).
[11] Pierce,A. K., Appl. Opt. **3** 1337-1346 (1964).
[12] Denker, C., et al., Proc SPIE **6267** (2006).
[13] Rimmele,T.R, Proc SPIE **5901**, 41-51 (2005).
[14] Storey,J., et al., Proc SPIE **6267** (2006).
[15] Moretto,G., and J.R. Kuhn, Appl. Opt., **39**, 2782-2789 (2000).
[16] Moretto,G., and J.R. Kuhn, Appl. Opt., **37**, 3539-3546 (1998).
[17] Kay,R.R., et al., Proc. SPIE **3753,** 347-355 (1999).
[18] Price, M.E., Proc. SPIE **4814,** 162-172 and 173-181 (2002).
[19] Figoski, J., Proc SPIE **3779** (1999).
[20] Lencione, D.E., et al., Proc SPIE **3870** (1999).
[21] Subrahmanyam, D., et al., Proc SPIE **6405** (2006).
[22] Perryman, M.A.C., Proc. GAIA Symposium ESA **SP-576**, 15-22, (2005).
[23] Graue, R., et al., Proc SPIE **4854** (2003).
[24] Krist, H., et al., Proc SPIE **4860** (2003).
[25] Noecker, C., Proc SPIE **4860** (2003).
[26] Trauger, J., et al., Proc SPIE **4854** (2003).
[27] Hull, T., et al., Proc SPIE **4860** (2003).
[28] Kuhn, J.R., et al., PASP **113,** 1486-1510 (2001).
[29] Kuhn, J.R., and S.L. Hawley, PASP **111,** 601-620 (1999).
[30] Chang Jun et al., Proc SPIE **4927** (2002).
[31] Chang Jun et al., Proc SPIE **5638** (2005).
[32] Rodgers, J.M., Proc SPIE **4832** (2002).
[33] Agurok, I., Proc SPIE **3779** (1999).
[34] Owen, R.C., Proc SPIE **1354** (1990).
[35] Hallam, K.L., et al., U.S.Patent 4,598,981 (1986).
[36] Jones, L.R., Proc SPIE **1762** (1992).
[37] Lampton, M., and M.Sholl, Proc SPIE **6687** #0S, (2007).
[38] Sholl, M., et al., Proc. SPIE **7691** #26 (2010).
[39] Korsch, D., Appl. Opt. **11** #12 (1972), **16** #8 (1977), and **19** #21 (1980).
[40] Cook, L.G., Proc SPIE **183,** 207-211 (1979).
[41] Bernstein, G., PASP **114,** 98-111 (2002).